Investigation of Antibacterial and Cytotoxicity Effect of Green Synthesized TiO_2 Nanocomposites, an Experimental and Theoretical Study

Khazaeli, Payam; Ranjbar, Mehdi
Pharmaceutics Research Center, Institute of Neuropharmacology, Kerman University of Medical Science, Kerman, I.R. IRAN

Ahmadi Zeidabadi, Meysam
Neuroscience Research Center, Institute of Neuropharmacology, Kerman University of Medical Science, Kerman, I.R. IRAN

Kalantar Neyestanaki, Davoud•
Medical Mycology and Bacteriology Research Center, Kerman University of Medical Sciences, Kerman, I.R. IRAN

Razavi, Razieh*+
Department of Chemistry, Faculty of Science, University of Jiroft. Jiroft, I.R. IRAN

Ziasistani, Mahsa
Pathology and Stem Cell Research Center, Afzalipour Hospital, Kerman University of Medical Science, Kerman, I.R. IRAN

Amiri, Mahnaz*+
Neuroscience Research Center, Institute of Neuropharmacology, Kerman University of Medical Science, Kerman, I.R. IRAN

ABSTRACT: *Protecting the hair, skin, or products of itself are utilized by sunscreen filters which were frequently blocked hazardous UV-Vis radiation. Considering its photoprotective impact on the skin facing the radiation of ultraviolet and visible, TiO_2 is a common and cost-efficient photocatalytic structure utilized in sunscreens. In this research, the continual process was done to optimize the green synthesis of TiO_2 nanoparticles and nanocomposites through a new, easy, cost-efficient, and quick approach to making nanostructures utilizing a sonochemistry method. SiO_2, Al_2O_3, ZnO, and MnO were utilized to compose green synthesized TiO_2 nanoparticles for this purpose. The samples were recognized by XRD, FT-IR, DLS, and SEM. Also, the cytotoxicity and antibacterial activity were assessed. DFT computation was performed to identify the connected energy and band gap energy of nanocomposites by B3LYP/Lan2DZ quantum approach. TiO_2/Al_2O_3 showed a lower size and the lowest agglomeration than synthesized TiO_2 and other nanocomposites. Furthermore, all samples indicated strong*

***** *To whom correspondence should be addressed.*
+ E-mail: ma.amiri@kmu.ac.ir ; r.razavi@ujiroft.ac.ir
● Other Address: Department of Microbiology and Virology, School of Medicine, Kerman University of Medical Sciences, Kerman, I.R. IRAN
1021-9986/2022/7/2189-2201 13/$/6.03

antibacterial activity against investigated bacteria due to cell death caused by membrane permeability increase and bacterial wall integrity disruption. Nanostructures have cytotoxicity with a low level on A172 cells. The only exception is TiO_2/ZnO which indicated a potent index of cytotoxicity on the cancerous cell lines as demonstrated by a low IC_{50} value of 50 ppm. The relative energy and band gap of nanocomposites indicated that TiO_2/Al_2O_3 has the best stability in chemical and biochemical mediums among other nanocomposites. These green synthesized TiO_2/Al_2O_3 nanostructures may have promising applications in nanoformulation to combat bacterial infections in the future.

KEYWORDS: *Titanium dioxide, Materials chemistry; Environmental friendly synthesis; TiO_2 nanocomposites; Antibacterial, DFT calculations.*

INTRODUCTION

Antioxidants and sunscreen compounds are products for skin protection that were paid attention to the health science. Hence, they can inhibit the skin's harmful and damaging impacts, involving cancers and intracellular imbalance between free radicals and human diseases. [1]. Ultraviolet-visible radiation is the most significant effect for disordering skin, like scaling, wrinkling, mottled pigment abnormalities, and dryness [2]. Thus, a significant element for healthcare products will be antioxidant action due to examining active oxygen types and extinguishing the speed of oxidative reactions. [1]. Low-energy UV-vis A (320–400 nm), high-energy UV-Vis B (280–320 nm), and UV-vis C (200–280 nm) are three band regions of hazardous ultraviolet-visible light [3]. The atmospheric ozone layer absorbs ultraviolet, visible C region which is less concerned from a health viewpoint. A wide difference in spatial sunscreen products was developed to avoid photodamage by UV-vis light. Two basic sorts of UV-vis filters are used as the active ingredient of sunscreen products. UV radiation wavelengths can be absorbed by organic filters due to their chemical structures. Titanium dioxide and zinc oxide as inorganic filters can absorb and scatter UV-vis radiation, and block UV-Vis domain more than the organic chemical blends. A sunscreen formulation focuses on the filters encapsulated physicochemical characteristics and the carrier [4]. TiO_2 crystalline polymorphic formulations are involved in rutile, anatase, and brookite [5], just the sunscreens were created by the rutile and anatase phases [6]. In comparison, the rutile is more permanent and has lower photocatalytic activity than anatase. TiO_2 primarily supports facing UV-Vis B rays which can protect against UV-Vis due to the size and distribution of particles [7]. Considering the versatile characteristics of NPs, involving surface area, particle size, and quantum impacts, NPs are highly utilized in commercial products [8]. TiO_2 NPs are basically utilized in personal-care products, coatings, cleaning agents, and paints, producing around 10,000 tons per year [9]. These wide and increasing productions also raise concerns based on the potential toxicity to living organisms [8] NPs can negatively impact human health by following both the human host and its microbiomes. *Escherichia coli* (*E. coli*) is observed as single-cell bacteria in the intestines of animals and humans in an aquatic environment. The prokaryotic organism is utilized in research and is an excellent host to produce multiple proteins. The study showed that the toxicity of TiO_2 NPs to *E. coli* is increased by small particle sizes and large surface areas [10]. Besides, the toxicity degree in E. coli was found to be affected by ionic strength and electrolytes which affect TiO_2 aggregation [11]. Although the amount of TiO_2 particles have a significant role in the function of this material in sunscreen formulations, the large size of these particles (> 200 nm) leads to a low efficacy against UV-Vis rays and displays visible light making an opaque film on the skin. On the other hand, fine particles (< 200 nm) are more transparent in visible light with broader refractive abilities and better support in the UV-Vis B range. TiO_2 powder with micro/nano size has a tendency to aggregate, resulting in products with low UV-Vis attenuation and weak aesthetic charactersitics [12]. The band gap of the TiO_2 is commonly a range of 3.0–3.2 eV and the wavelength is about 400 nm. This means that UV light radiation with a wavelength of less than 400 nm can stimulate the electrons and initiate a photo-reaction[13].The approaches for extending the colloidal fixation of TiO_2 particles must be applied to delete the tasteful drawback. A method to do the photocatalytic activity and increase the particles' colloidal stability is TiO_2 surface coating with inorganic or natural compounds [14]. For example, the particles will be coated with inorganic layers

, such as silica [15], alumina [16], and zirconia [17], or natural polymers such as sodium polyacrylate [18], spray-drying[19], solvothermal[20], microwave[21], and sol-gel course[22] methods were utilized for coating the TiO2 particles. Hence, these strategies apply high temperatures and long reaction times which may increase the final product cost. A sonochemistry approach not only does not need high temperatures but also a long reaction time, but has the ability to produce hotspots with 5000 °K and 1000 atm, therefore is a complete approach for coating TiO_2 Nanostructures[23] The cause is developing those synthesis environments for nanomaterials that are clean, humble, and environmental-friendly methods to decline or delete applying chemical products as well as producing safe materials [24].

Making a novel, quick, and simple approach to the synthesis od TiO_2 nanoparticles and nanocomposites in the existence of a green antecedent as a capping and soluble agent was among the targets of this research. The synthesized particles were evaluated as an inorganic channel for sunscreen definitions. X-Ray powder Diffraction (XRD), Fourier Transform InfraRed Spectra (FT-IR), Scanning Electron Microscopy (SEM), Zeta potential (ζ), Dynamic Light Scattering (DLS), Transmission Electron Microscopy (TEM) and Density Functional Theory (DFT), frequently discovered the created materials. The cytotoxicity and antibacterial impacts of formulations were assessed.

EXPERIMENTAL SECTION

Materials and chemicals;

The whole chemicals and reagents utilized here were analytical grade (purity≥99%) and applied with no more purification. Titanium chloride ($TiCl_4$, analytical grade, purity≥99.85%) was used as a precursor straightforwardly with no more purification for the synthesis of TiO_2 NPs. Commercial TiO_2 was prepared by Tecnan company (Spain) which used it to contrast with green synthesized TiO_2. Green tea leaves are utilized for the green synthesis of TiO_2 NPs. Twofold Distilled Water (DW) was used in the whole test.

Green synthesis of TiO_2 NPs

Initially, using DW water, green tea leaves were precisely washed to expel the connected dust particles and cut into so fine pieces and dried in sunlight. 20.0 g of leaves were submerged in 100 mL of DW water and boiled at 80 °C for 40 min to prepare leaf extract. Hence, the provided leaf extract was kept for cooling at room temperature, and filtered utilizing Whatman filter paper which was utilized for the green synthesis of TiO_2 NPs. For the green synthesis of TiO_2 NPs, $TiCl_4$ powder was poured into the beaker and diluted with 80 mL of distilled water. Leaf extract with a ratio of 1:1 toward TiCl4 was added. After 20 min continuous stirring at room temperature, the solution color changed from transparent to whitish-brown. The observed color change indicated the reduction of metallic particles (Ti^{4+}) which showed the green synthesis of TiO_2 NPs. For accelerating the NPs, 5 mL of ammonia was involved in the solution of NPs drop-wise beneath nonstop stirring at room temperature. Thus, the precipitates taken from NPs were separated from the solution through filtration, by washing with ethyl alcohol to evacuate the ionic impurities. Hence, the washed precipitates were air-dried and calcined at 450 °C for 3 h and at last grind in a crystal mortar pestle to take the ultimate powder form of TiO_2 NPs. The schematic of green synthesis TiO_2 nanostructures is displayed in Fig. 1. and the feasible reaction mechanism is present in Fig. 2 [25].

Synthesis of TiO_2 nanocomposites

The used amount of TiO_2, Ethanol, H_2O, and NH_4OH for all samples was in the ratio of 1g/15.3 mL /24 mL /0.2 mL, respectively. Initially, green synthesized TiO_2 scattered in ethanol and water and composite agents added and the final solution was set in ultrasound (Hielscher Ultrasonic Disruptor; 20 kHz; 675 W) for 5 min, and NH_4OH was gradually added at the final of 4 min. The precipitation particles were washed with water and ethanol *via* centrifuged at 3500 rpm for 15 min by evacuating an abundance of NH_4OH. This process was repeated until the pH of the supernatant comes to an unbiased pH. At last, the samples dried in an oven at 70 °C. The used composite agents were tetraethyl orthosilicate (TEOS), aluminum nitrate, zinc chloride, and manganese chloride for the synthesis of TiO_2/SiO_2, TiO_2/Al_2O_3, TiO_2/ZnO, and TiO_2/MnO, nanocomposites respectively.

In vitro cytotoxicity assay

By MTT dye diminishing, the rate of the viable cell was in a roundabout way identified in which MTT was decreased by dynamic mitochondria in living cells [26]. As *Sladowski et al.*

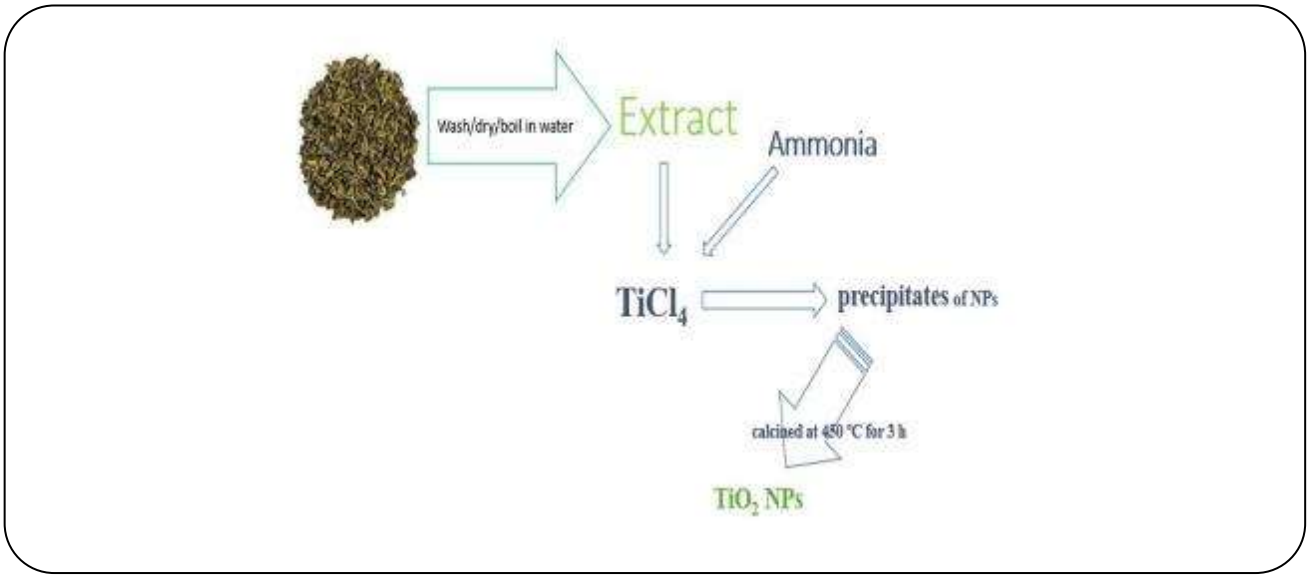

Fig. 1: The schematic of green synthesis TiO_2 nanostructure.

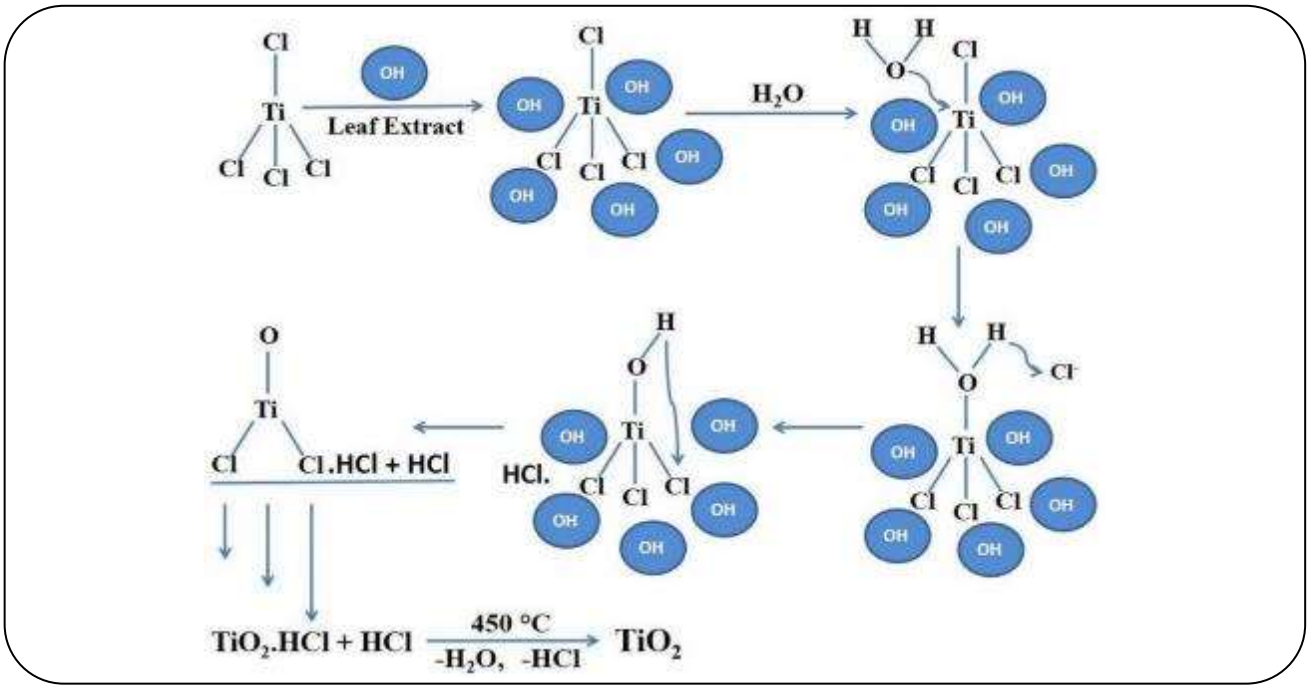

Fig. 2: Possible reaction mechanism of green synthesis of TiO2 NPs [26].

noted, the MTT measure was handled to the balanced strategy [27]. 2 × 102 cells were incubated in 96-well plates (Iwaki) with 1 mg/mL of MTT in DMEM at 37 °C and 5% CO2 for 2 h. The cells were at that point washed three times with 0.2-M phosphate buffer saline (PBS) at pH 7.4, and the decreased MTT formazan crystals were solubilized in 250 mL of DMSO. The Optic Density (OD) was perused at 570 nm by an Enzyme-Linked ImmunoSorbent Anaylys (ELISA) peruser (Pharmacia Biotech, Stockholm, Sweden). The rate of dead and live cells was calculated considering control that reveals the cytotoxicity of each treatment, as suggested by *Zhang et al.* [28] as follows: % of cellular viability = (Abs of sample − Abs of blank) /(Abs of control− Abs of blank) × 100

The concentration which promotes the decrease of 50% in the cellular viability (IC50) was computed by the linear regression of curve dose versus reaction, for multiple concentrations of nanocomposites.

Antibacterial investigations

Staphylococcus epidermidis, Pseudomonas aeruginosa ATCC 27853and *Escherichia coli* ATCC 25922 were grown on peptone-broth at 37 °C in a shaker incubator. After 24h, 20 microliters of Liquid cultures were diluted in 96 culture plates containing 200 microliter broth medium. The different concentrations of TiO_2 NPS such as 31.25, 62.5,125, 250, and 500µg/mL added. The turbidity of Overnight cultures was evaluated at 530 nm and compared by the control group [29].

Characterization of green synthesized TiO_2 Nanocomposites

The synthesized tests were identified by a series of technologies involving X-Ray Diffraction (XRD) patterns which were recorded by a Philips-X'pertpro, X-Ray Diffractometer utilizing Ni-filtered Cu Ka radiation. Fourier transform infrared (FT-IR) spectra were registered on Bruker, FT-IR alpha model. Utilizing an FE-SEM, ZEISS, SIGMA VP-500, Germany). Identifying particle size was done by Nanosizer cordovan (France), and produced MNPs morphologies were surveyed. UV/Visible Spectrophotometer (Optizen 3220, Korea) applied for ultraviolent detection.

Statistical analysis

Applying statistical package for social science (SPSS) version 16 software (IBM, Armonk, NY, USA), data analysis was done. Data were displayed as the mean Standard Error of the Mean (SEM). Significance between treated vs. control groups was shown by the t-Student's test at 95% confidence. P-values less than 0.05 were shown critically.

Theoretical method

To indicate relative energy and band gap, DFT analysis was done by B3LYP/Lan2DZ in Gaussian 09 software package [30].

Results and discussion

Characteristics of green synthesized TiO_2 NPs and nanocomposites

FT-IR analysis

FT-IR prepares data considering the existence of beneficial groups and features of molecular bonds in the substance. FT-IR spectra of green synthesized TiO_2 nanoparticles, commercial TiO_2, and TiO_2 nanocomposites which are present in Fig. 3. All tests indicate the existence of water and hydroxyl bunches by bowing vibration of H–O–H at 1600 cm^{-1} and a solid extending vibration of O–H at 3500 cm^{-1} [31]. The band at 500–700 cm^{-1} is seen in overall tests allotted to Ti–O–Ti [32]. In the FT-IR spectra of TiO_2 nanoparticles, ultrasound does not deliver a distinguishable alter. Hence, due to the existence of coating specialists, coated tests revealed extra groups. TiO_2@SiO_2 test contrasted the spectrum of non-coated TiO2 indicates abroad band in the domain of 850 cm^{-1} related to the deviated extending vibration of Si-O-Si group [31]. Hence, the band at 1100 cm_{-1} within the test TiO_2/Al_2O_3 has ascribed to Al–O extending vibration [33]. This peak of vibration of H–O–H for TiO_2/ZnO and TiO_2/Mno was observed at 1630 and 1695 cm^{-1}, respectively.

SEM, TEM, and DLS analysis

By measuring the particle size from DLS strategy of nanosized estimation, the particle size distribution curves were prepared. Fig.4 indicates the synthesized sample size determined by DLS nanosized. Table 1 displays the hydrodynamic size provided due to DLS measurements. The samples of TiO_2/SiO_2, TiO_2/MnO, and green synthesized TiO_2 show high hydrodynamic size (823 nm, 786 nm, and 786 nm, respectively), this increasing size is related to agglomerate arrangement and exceptionally wide measure dispersion. Hence, the hydrodynamic size of commercial TiO_2 (653 nm) and TiO_2/Al_2O_3 is the last one, nearly 595 nm, TiO_2/ZnO shown 684 nm. The ultrasonic vitality input applied to break down the particle aggregates [17], the ultrasonic energy did not influence amazingly. TiO_2 nanostructures are Spherical, TiO_2/Al_2O_3 and TiO_2/ZnO were found to be globular with complete grains that are obvious in SEM images, these results indicated that ultrasound and the coating process did not alter the morphology of samples (Fig. 5). SEM applied to make high-resolution images for better understanding of different coating (Al_2O_3, ZnO, MnO and tetraethylorthosilicate (TEOS)) on green synthesized TiO_2 NPs. The results indicate that in Al_2O_3 and ZnO nanostructures a uniform distribution of particles is observed in MnO and TEOS agglomeration zone takes place seeing the dynamic surface of nanoparticles. Fig.6 presents Transmission Electron Microscopy (TEM) of TiO_2/Al_2O_3 nanocomposites in this figure, it is obvious that the real size of synthesized TiO_2/Al_2O_3 the nanocomposite is

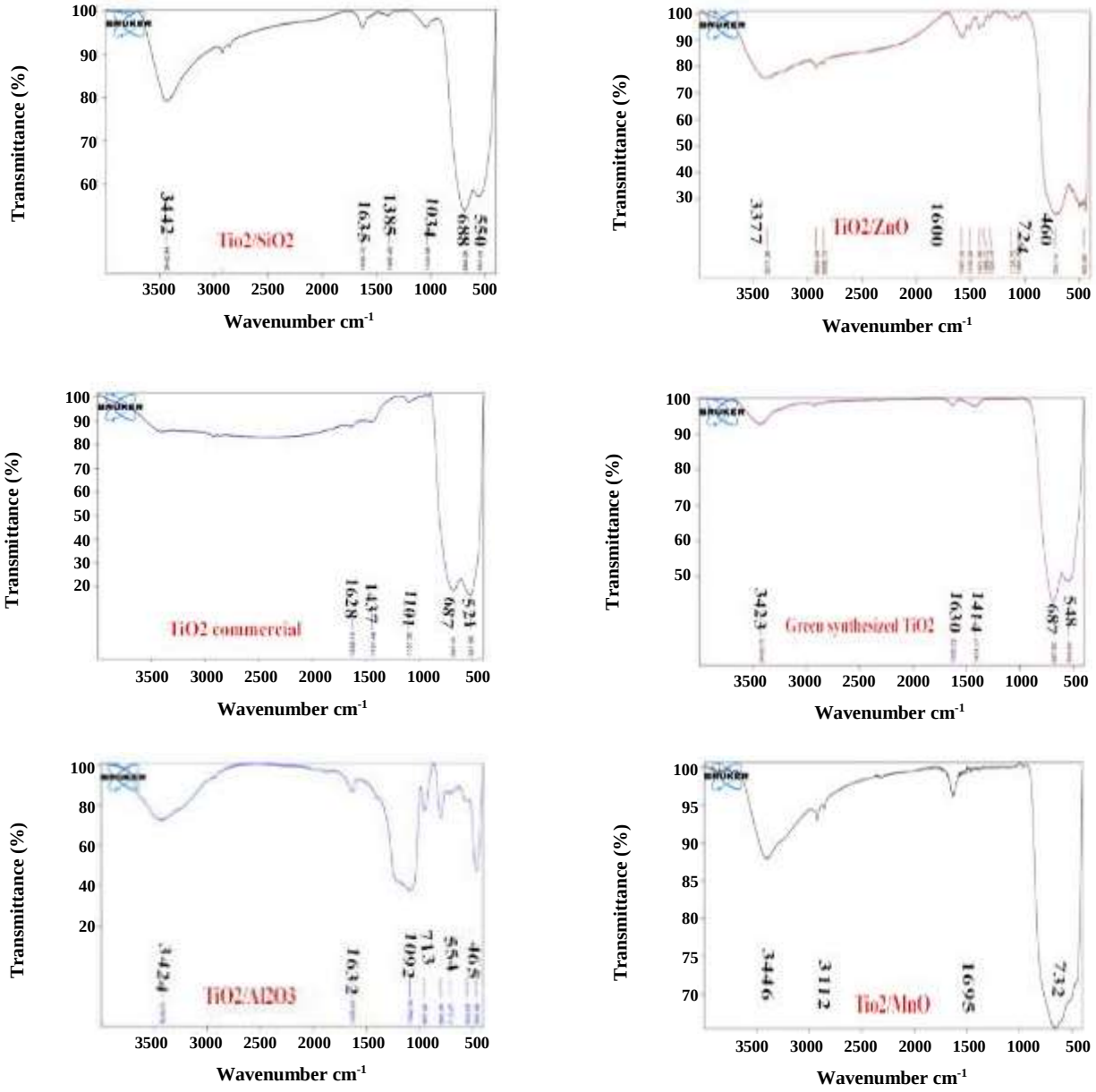

Fig. 3: The FT-IR spectrum of green synthesized TiO_2/SiO_2, TiO_2/Al_2O_3, TiO_2/ZnO, and TiO_2/MnO nanocomposites.

around 100 nm this size is because of the hydrodynamic diameter remove in TEM images. At the end of Table 1, the size of nanoparticles was compared with other related papers.

XRD analysis

Assessing the crystalline structure of green synthesized TiO_2, XRD analysis was done and the most excellent composing nanoparticles revealed less size after DLS measurement. Fig. 5 indicates the XRD patterns of green synthesized TiO_2 and TiO_2/Al_2O_3 nanocomposites. In 2θ=25°, 27°, 36°, 37°, 41°, 48°, 56°, 62° ,69°,70° and 75° for green synthesized sample. The observed peaks 25° can be ordered as rutile stage (space bunch P42/mnm, reference code 01-084-1284). The small peak at 2θ=27° (Fig. 7(A)) is allotted to the anatase step of TiO_2 (space bunch I41/amd, reference code 01-071-1167). Hence, the present peak vanishes passing sonication and coating steps (Fig. 7(B), hence it is hard to identify anatase TiO_2 existence by XRPD when its substance is less than 5% wt [37].

Table 1: The nanocomposite size determined by DLS nanosizer.

Sample no	Nanocomposiote	Size (nm) Di90%
1	TiO_2/Al_2O_3	595±10.56
2	TiO_2/ ZnO	684±6.65
3	TiO_2/ MnO	786±4.99
4	TiO_2/ SiO2	823±5.16
5	$TiO_{2\ (work)}$	786±6.53
6	$TiO_{2(commercial)}$	653±6.38
[34]	TiO2/Al2O3	1367.66 ± 254.26
[35]	TiO2 NPS	50nm 2 micrometer
[36]	TiO2 NPS	10-20 nm

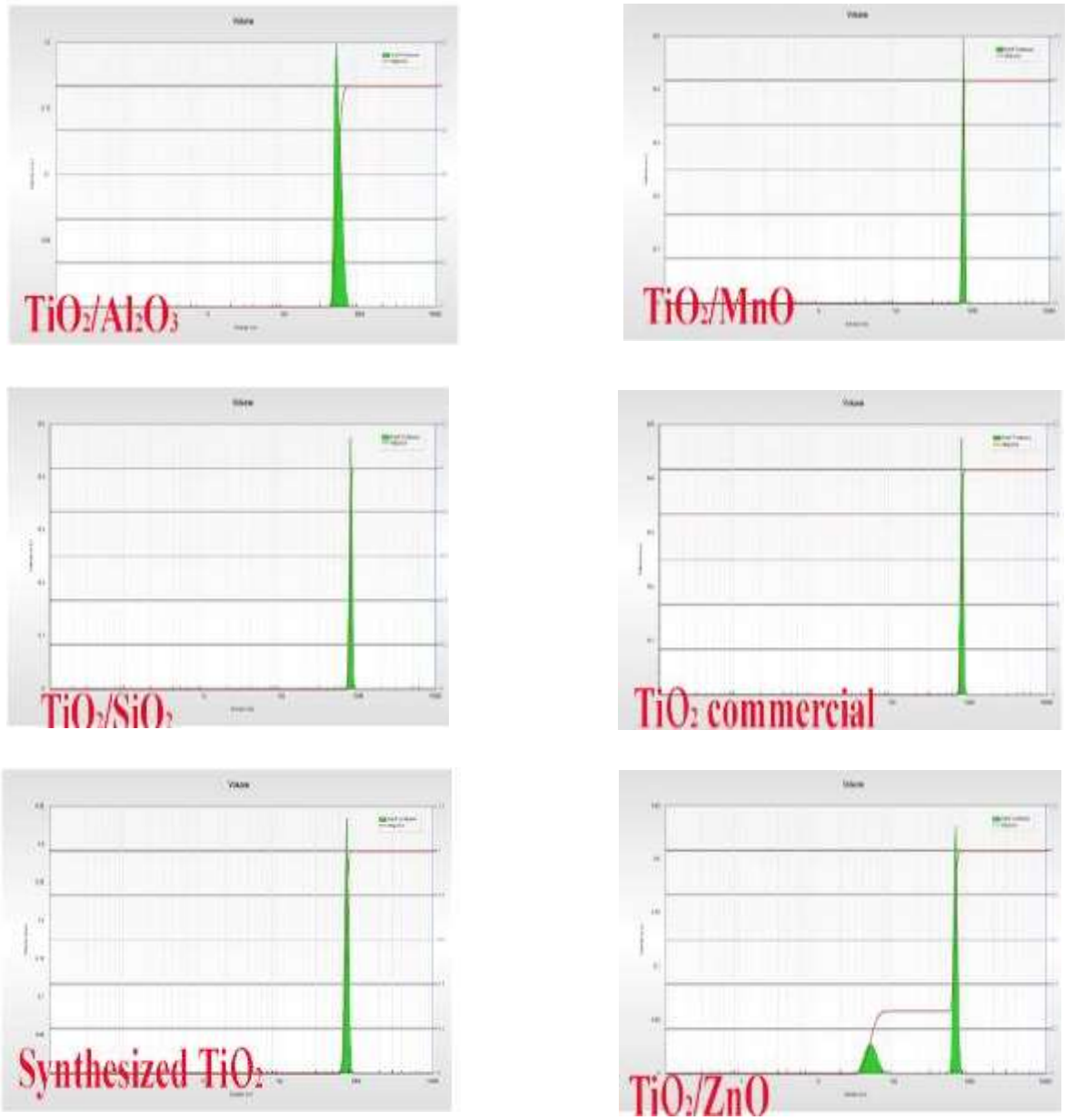

Fig. 4: The synthesized sample size determined by DLS nanosized.

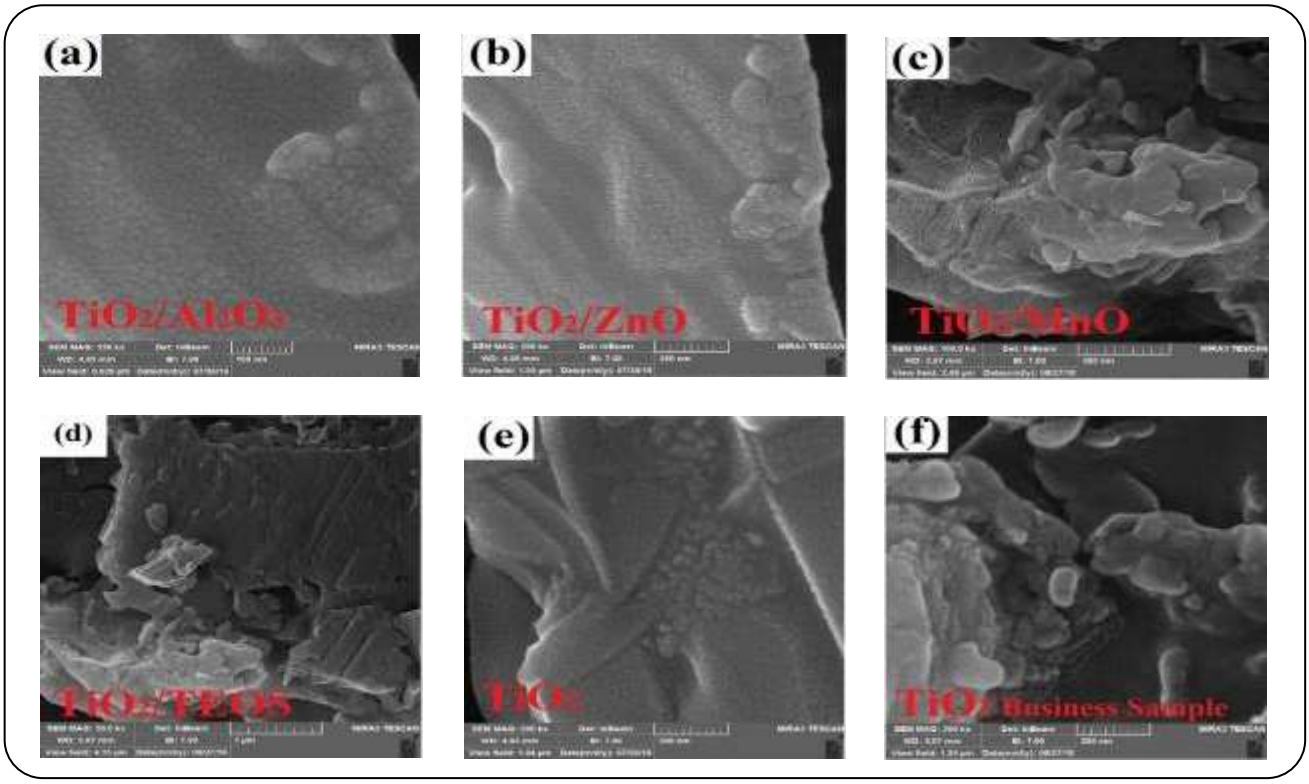

Fig. 5: Scanning electron microscopy (SEM) of TiO_2 NPs , nanocomposites and commercial TiO_2 nanostructure.

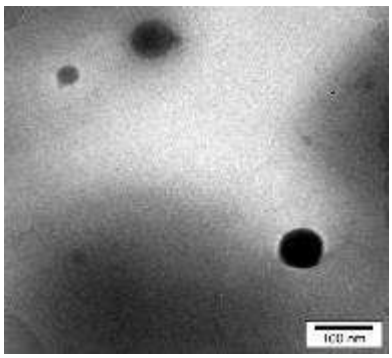

Fig. 6. Transmission electron microscopy (TEM) of TiO_2 /Al2O3 nanocomposites

Moreover, extra peaks were not seen in overall coated tests. It indicates the coating materials are in a nebulous stage or in little amounts to be recognized by XRPD [38].

MTT Investigations

Among major concerns for synthesized nanoparticles in biomedical utilizations, we can note security and poisonous quality. To assess the cytotoxic impacts of multiple nanoparticles, and results revealed that the cytotoxicity may be due to different variables, multiple research was done. Also, to assess the cytotoxicity impact of the green synthesized TiO_2 nanostructures and different nanocomposites on A172 cell line, MTT assays were utilized. The cells were incubated at 37 °C for 24 h beneath multiple test concentrations. As shown in Fig.8, the cell viability maintained 80% after 24 h of treatment with nanostructures at a concentration as high as 100 µg/mL for all nanoparticles except for TiO_2/ZnO which reached 60%. Zinc oxide (ZnO) is a metal oxide semiconductor that has been used widely for different applications [37]. The above diagram indicates that as-prepared nanostructures have a low level of cytotoxicity on A172 cell lines. The only exception is TiO_2/ZnO. About 50 µg/ mL of this substance has caused the death of 50% of cells. The high cell viability in all concentrations is attributed to the biocompatibility of the synthesized nanostructures. Therefore, due to the obtained data, the synthesized different kinds of TiO_2 nanocomposites are a promising candidate for various biomedical applications.

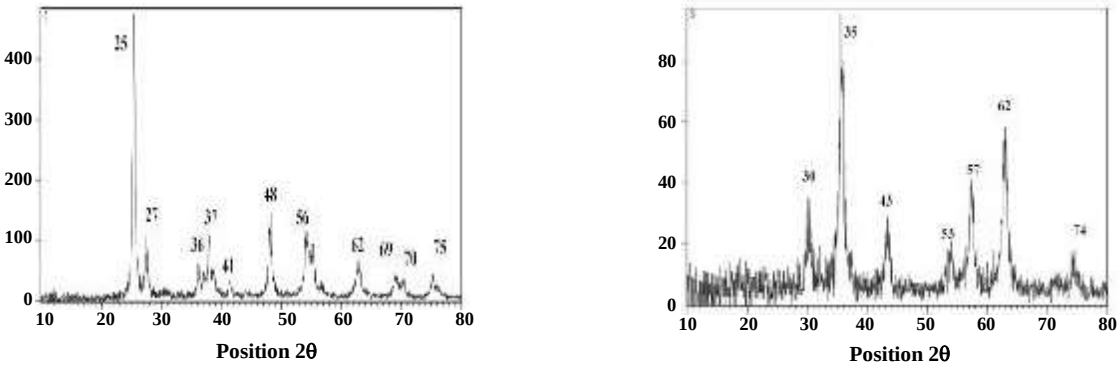

Fig. 7: The X-ray diffraction pattern of green synthesized TiO2 nanostructures (the first)and TiO_2/Al_2O_3 nanocomposite (the second).

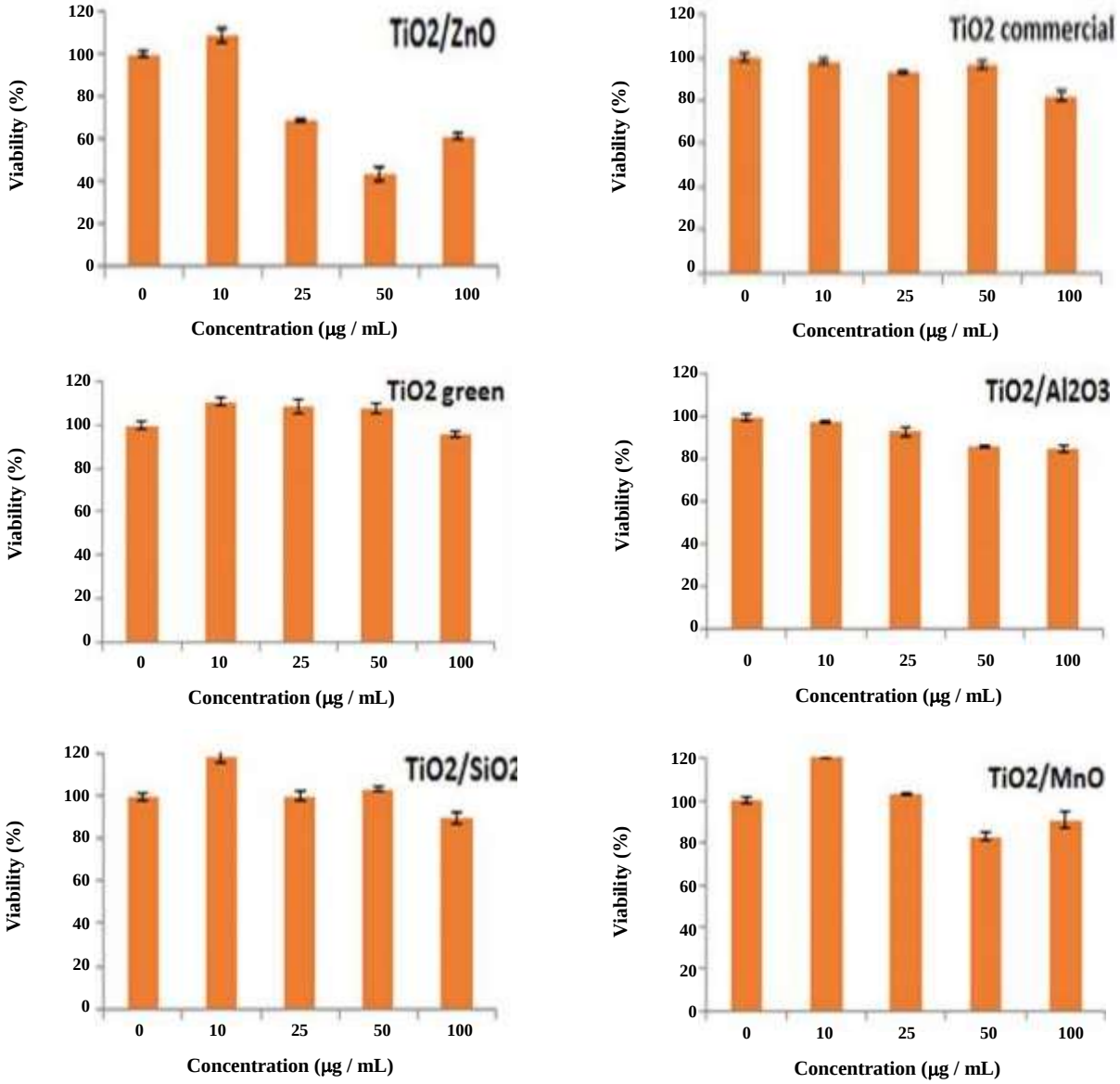

Fig. 8: The cytotoxicity investigation of various nanocomposites in cell lines.

Table 2: Relative energy, HOMO, and LUMO of nanocomposites

Nanocomposite	ΔE(a.u.)	HOMO(a.u.)	LUMO(a.u.)
TiO2@Al2O3	-0.134	-0.18795	-0.14854
TiO2@ZnO	-0.0548	-0.17558	-0.16586
TiO2@MnO	-0.0394	-0.16289	-0.16041
TiO2@SiO2	+75.119	-0.16928	-0.16310

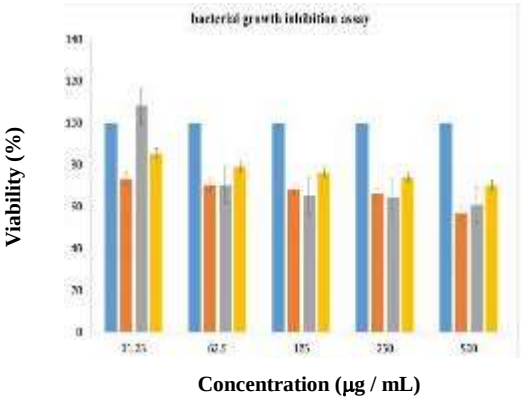

Fig. 9: The mortality (%) of the various concentrations of green synthesized TiO_2 nanoparticles on the different bacteria.

Antibacterial Activity

Staphylococcus epidermidis, *Pseudomonas aeruginosa*, and *Escherichia coli* were grown on peptone-broth at 37 °C in a shaker incubator. After 24h, 20 microliters of liquid cultures (broth) were diluted in 96 culture plates containing 200 microliter broth medium. We added different concentrations, such as 31.25, 62.5,125, 250, and 500 of TiO^2. The turbidity of Overnight cultures was evaluated at 530 nM and compared by the control group. It is obvious from Fig. 9 that the synthesized nanocomposite indicated strong antibacterial activity against investigated bacteria due to cell death caused by membrane permeability increase and bacterial wall integrity disruption.

DFT Calculations

An important role of theoretical calculation is estimating and calculating the stability, present ability, and chemical properties of chemical compounds. Since TiO_2 nanocomposite was synthesized to obtain the stability of relative energy, all chemical compounds were optimized. Lattice crystals of TiO_2, SiO_2, MnO, Al_2O_3, and ZnO were used. Two connection sides of TiO_2 with other compounds were satisfied O connector side and Ti connector side. Fig. 10 indicated the active side of connecting nanocomposites. The relative energy of each nanocomposite was plotted in Fig. 11. Due to the reported data relative energy of $TiO_2@Al_2O_3$ is -0.134 a.u and TiO_2@ZnO, TiO_2@Mno, and $TiO_2@SiO_2$ are -0.0548,-0.0394 and +75.119 a.u. respectively. $TiO_2@Al_2O_3$ has less energy than the other nanocomposites; therefore, it is the most stable synthesized nanocomposite. The density and distribution of electrons on the surface or ground of atoms and molecules can result in the chemical reactivity of atoms or molecules. Important facilities of a chemical compound to modify the chemical parameters are HOMO and LUMO. In Fig. 12, HOMO and LUMO of nanocomposites were demonstrated to recognize negative (red) and positive (green) nanocomposite places. The value of HOMO and LUMO and bandgap (ΔE) of nanocomposites' energy are presented in Table 1. The value of HOMO and LUMO and bandgap (ΔE) of nanocomposites' energy are presented in Table 2. If the bandgap is more negative caused high and best reactivity in chemical and biochemical media [33]. Amount -0.0395 a.u. for a bandgap of $TiO_2@Al_2O_3$ expresses these nanocomposites have the best chemical reactivity.

CONCLUSIONS

The sonochemical method used for green synthesized TiO_2 nanocomposites with different materials like SiO_2, Al_2O_3, ZnO, and MnO to synthesize various nanocomposites TiO_2/Al_2O_3, TiO_2/SiO_2, and TiO_2/MnO, and TiO_2/ZnO. Among nanocomposites, TiO_2/Al_2O_3 indicated lower agglomeration, the lowest size, and the best chemical reactivity with antibacterial activity for biomedical applications. All samples indicated strong antibacterial activity against investigated bacteria due to cell death caused by membrane permeability increase and bacterial wall integrity disruption. Nanostructures have cytotoxicity with a low level on A172 cells. DFT computation was performed

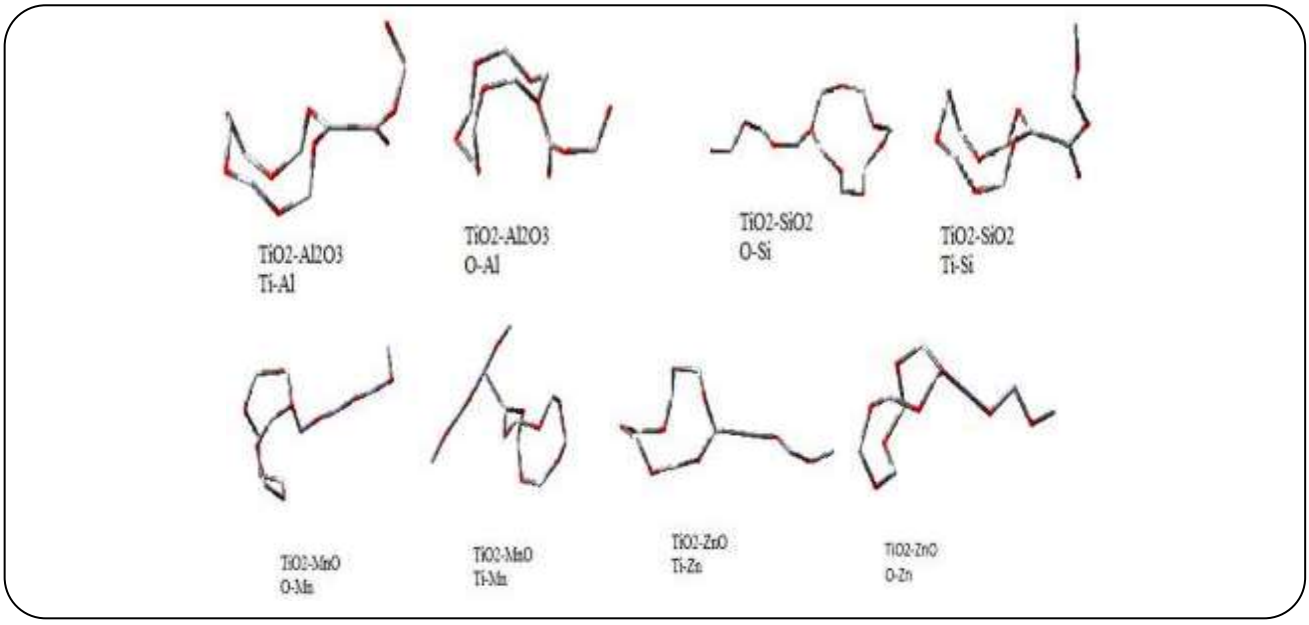

Fig. 10: Nano composites Structure in O connection and Ti connection.

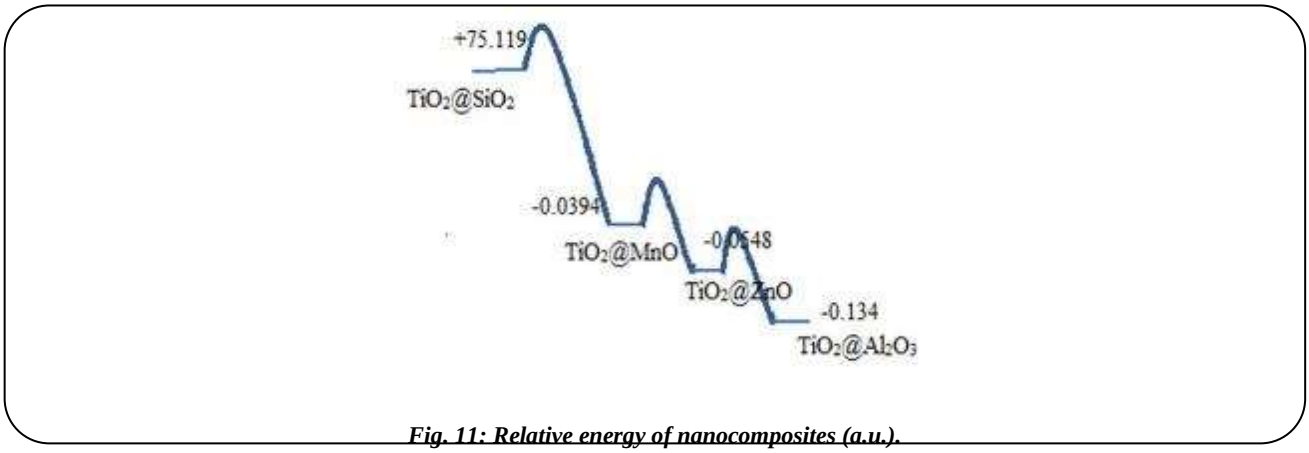

Fig. 11: Relative energy of nanocomposites (a.u.).

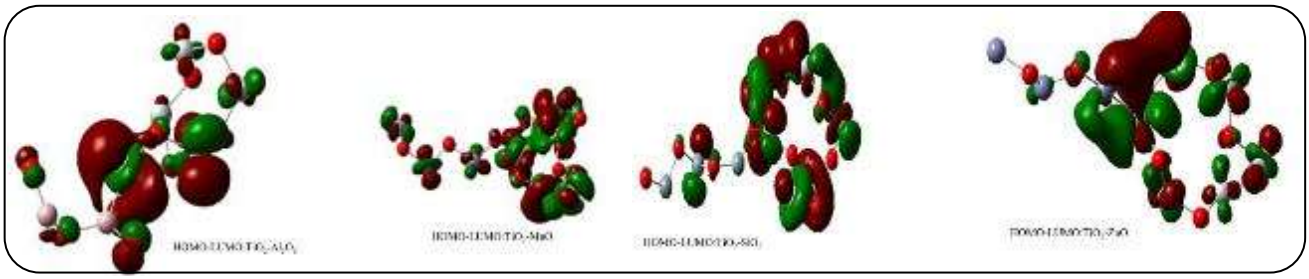

Fig. 12: HOMO and LUMO distribution of nanocomposites

to identify the connected energy and band gap energy of nanocomposites by B3LYP/Lan2DZ quantum approach. The present study indicates that the suggested sonochemistry approach can improve the TiO_2 characteristics in an easy method and short period, also shows the significance of this ultrafast and effective methodology which is still unknown in-cosmetics utilizations.

Received : May 31, 2021 ; Accepted : Sep. 14, 2021

REFERENCES

[1] Devasagayam T.P.A., Tilak J.C., Boloor K.K., Sane K.S., Ghaskadbi S.S., Lele R.D., Free Radicals and Antioxidants in Human Health, *J. Assoc. Physicians India*, **52**: 794 (2004).

[2] Nichols J.A., Katiyar S.K., Skin Photoprotection by Natural Polyphenols: Anti-Inflammatory, Antioxidant and DNA Repair Mechanism, *Arch. Dermatol. Res.*, **302**: 71 (2010).

[3] Czégény G., Wu M., Dér A., Eriksson L.A., Strid Å., Hideg É., Hydrogen Peroxide Contributes to the ultraviolet-B (280–315 nm) Induced Oxidative Stress of Plant Leaves Through Multiple Pathways, *FEBS Lett.*, **588**: 2255 (2014).

[4] J. S.K. and J. N.K., Lipopeptides in Cosmetics, *Int. J. Cosmet. Sci.*, **32**: 89 (2010).

[5] Lu P.J., Huang S.C., Chen Y.P., Chiueh L.C., Shih D.Y.C., Analysis of Titanium Dioxide and Zinc Oxide Nanoparticles in Cosmetics, *J. Food Drug Anal.* **23**: 587 (2015).

[6] Wu D., Mao F., Yang Z., Wang S., Zhou Z., Enhanced Osteogenic Activity of Ti Alloy Implants by Modulating Strontium Configuration in their Surface Oxide Layers, *Mater. Sci. Semicond. Process.*, **23**: 72 (2014).

[7] Manaia E.B., Kaminski R.C.K., Corrêa M.A., Chiavacci L.A., Ultraviolet Protection Properties of Commercial Sunscreens and Sunscreens Containing ZnO Nanorods, *Brazilian J. Pharm. Sci.*, **49**: 201 (2013).

[8] Wang S.Q., Lim H.W., Principles and Practice of Photoprotection, *Princ. Pract. Photoprotection*, 1 (2016).

[9] Kyung Jeon S., Ju Kim E., Lee J., Lee S., Potential Risks of TiO_2 and ZnO Nanoparticles Released from Sunscreens into Outdoor Swimming Pools, *J. Hazard. Mater.*, **317**: 312 (2016).

[10] Piccinno F., Gottschalk F., Seeger S., Nowack B., Industrial Production Quantities and Uses of Ten Engineered Nanomaterials in Europe and the World, *J. Nanoparticle Res.*, **14**: (2012).

[11] Smijs T.G., Pavel S., Industrial Production Quantities and Uses of Ten Engineered Nanomaterials in Europe and the World, *Nanotechnol. Sci. Appl.*, **4**: 95 (2011).

[12] Lewicka Z.A., Benedetto A.F., Benoit D.N., Yu W.W., Fortner J.D., Colvin V.L., The Structure, Composition, and Dimensions of TiO_2 and ZnO Nanomaterials in Commercial Sunscreens, *J. Nanoparticle Res.*, **13**: 3607 (2011).

[13] Lahijani B., Hedayati K., Goodarzi M., Magnetic $PbFe_{12}O_{19}$-TiO_2 Nanocomposites and Their Photocatalytic Performance in the Removal of Toxic Pollutants, *Main Group Metal Chemistry*, **41 (3-4)**: 53-62 (2018).

[14] Egerton T.A., Tooley I.R., UV Absorption and Scattering Properties of Inorganic- Based Sunscreens, *Int. J. Cosmet. Sci.*, **34**: 117 (2012).

[15] Verma R., Awasthi A., Singh P., Srivastava R., Sheng H., Wen J., Miller D.J., Srivastava A.K., Interactions of Titania Based Nanoparticles with Silica and Green Tea: Photo-Degradation and Luminescence, *J. Colloid Interface Sci.*, **475**: 82-95 (2016).

[16] El-Toni A.M., Yin S., Sato T., Ghannam T., Al-Hoshan M., Al-Salhi M., Investigation of Photocatalytic Activity and UV-Shielding Properties for Silica Coated Titania Nanoparticles by Solvothermal Coating, *J. Alloys Compd.*, **508**: L1-L4 (2010).

[17] Liu Y., Zhang Y., Ge C., Yin H., Wang A., Ren M., Feng H., Chen J., Jiang T., Yu L., Evolution Mechanism of Alumina Coating Layer on Rutile TiO2 Powders and the Pigmentary Properties, *Appl. Surf. Sci.*, **255**: 7427 (2009).

[18] Zhang Y., Yin H., Wang A., Liu C., Yu L., Jiang T., Hang Y., Evolution of Zirconia Coating Layer on Rutile TiO2 Surface and the Pigmentary Property, *J. Phys. Chem. Solids*, **71**: 1458 (2010).

[19] Lee W.A., Pernodet N., Li B., Lin C.H., Hatchwell E., Rafailovich M. H., Multicomponent Polymer Coating to Block Photocatalytic Activity of TiO_2 Nanoparticles, *Chem. Commun.*, 4815 (2007).

[20] Morlando A., Sencadas V., Cardillo D., Konstantinov K., Suppression of the Photocatalytic Activity of TiO_2 Nanoparticles Encapsulated by Chitosan Through a Spray-Drying Method with Potential for Use in Sunblocking, *Powder Technol.*, **329**: 252 (2018).

[21] Yang L., Wang C., Liu Z., Liu X., Song Y., Feng X., Zhang B., Functionalizing Slag Wool Fbers with Photocatalytic Activity by Anatase TiO_2 and CTAB Modification, *Ceram. Int.*, **44**: 5842 (2018).

[22] Siddiquey I.A., Furusawa T., Sato M., Suzuki N., Microwave-Assisted Silica Coating and Photocatalytic Activities of ZnO nanoparticles, *Mater. Res. Bull.*, **43**: 3416 (2008).

[23] Rahim S., Sasani Ghamsari M., Radiman S., Surface Modification of Titanium Oxide Nanocrystals with PEG, *Sci. Iran.*, **19**: 948 (2012).

[24] Feng X., Zhang S., Lou X., Controlling Silica Coating thickness on TiO2 Nanoparticles for Effective Photodynamic Therapy, *Colloids Surfaces B Biointerfaces*, **107**: 220 (2013).

[25] Hangxun X., Zeiger B.W., Suslick K.S., Sonochemical Synthesis of Nanomaterials, *Chem. Soc. Rev.*, **42**: 2555 (2013).

[26] Amiri M., Pardakhti A., Ahmadi-Zeidabadi M., Akbari A., Salavati-Niasari M., Magnetic nickel Ferrite Nanoparticles: Green Synthesis by Urtica and Therapeutic Effect of Frequency Magnetic Field on Creating Cytotoxic Response in Neural Cell Lines, *Colloids Surfaces B Biointerfaces*, **172**: 244 (2018).

[27] Sadowski D., Steer S.J., Clothier R.H., Balls M., An Improved MIT Assay, *J. Immunol. Methods*, **157**: 203 (1993).

[28] Zhang T.Y., Wu, L., Tashiro S., Onodera S., Ikejima, Activation of Extracellular Signal-Regulated Kinase During Silibinin-Protected, Isoproterenol-Induced Apoptosis in Rat Cardiac Myocytes Is Tyrosine Kinase Pathway, *Acta Pharm.*, **25**, (2004).

[29] Kubacka A., Suárez Diez M., Rojo D., Bargiela R., Ciordia S., Zapico I., Albar J.P., Barbas C., Understanding the Antimicrobial Mechanism of TiO2-Based Nanocomposite Films in a Pathogenic Bacterium, *Sci. Rep.*, **4**: (2014).

[30] Frisch G.E.S.M.J., Trucks G.W., Schlegel H.B., Robb B.M.M.A., Cheeseman J.R., Scalmani G., Barone V., Petersson H.P.H.G.A., Nakatsuji H., Caricato M., Li X., Izmaylov M.H.A.F., Bloino J., Zheng G., Sonnenberg J.L., Ehara T.N.M., Toyota K., Fukuda R., Hasegawa J., Ishida M., Honda J.Y., Kitao O., Nakai H., Vreven T., Montgomery J. A., Peralta E.B.J.E., Ogliaro F., Bearpark M., Heyd J.J., Kudin J.N.K.N., Staroverov V.N., Kobayashi R., Raghavachari J.T.K., Rendell A., Burant J.C., Iyengar S.S., Cossi J.B.C.M., Rega N., Millam J.M., Klene M., Knox J.E., Bakken R.E.S.V., Adamo C., Jaramillo J., Gomperts R., Yazyev J.W.O.O., Austin A.J., Cammi R., Pomelli C., Martin G.A.V.R.L., Morokuma K., Zakrzewski V.G., Salvador A.D.D.P., Dannenberg J.J., Dapprich S., Farkas J.C.O., Foresman J.B., Ortiz J.V., Fox D.J., (n.d.).

[31] Niculae G., Lacatusu I., Bors A., Stan R., Photostability Enhancement by Encapsulation of α-Tocopherol Into Lipid-Based Nanoparticles Loaded with a UV Filter, *Comptes Rendus. Chim.*, **17**: 1028 (2014).

[32] Siddiquey I.A., Furusawa T., Sato M., Bahadur N. M., Mahbubul Alam M., Suzuki N., Sonochemical Synthesis, Photocatalytic Activity and Optical Properties of Silica Coated ZnO Nanoparticles, *Ultrason. Sonochem.* **19**: 750 (2012).

[33] Furusawa T., Honda K., Ukaji E., Sato M., Suzuki N., Multiwall Carbon Nanotube and TiO_2 Sol Assembly, *Mater. Res. Bull.*, **43**:946 (2008).

[34] Mahbubul I. M., Elcioglu E. B., Saidur R., Amalina M.A., Optimization of Ultrasonication Period for Better Dispersion and Stability of TiO_2–water Nanofluid, *Ultrason. Sonochem.*, **37**, 360 (2017).

[35] Zhang J., Yan S., Fu L., Wang F., Yuan M., Luo G., Xu Q., Wang X., Li C., Cuihua Xuebao/Chinese Photocatalytic degradation of rhodamine B on anatase, rutile, and brookite TiO_2, *J. Catal.* **32**, 983 (2011).

[36] X. Hangxun, B. W. Zeiger, and K. S. Suslick, Sonochemical Synthesis of Nanomaterials, Chem. Soc. Rev. **42**, 2555 (2013).

[37] Mahbubul I. M., Elcioglu E.B., Saidur R., Amalina M.A., Optimization of Ultrasonication Period for Better Dispersion and Stability of TiO_2–Water Nanofluid, *Ultrason. Sonochem.* **37**: 360 (2017).

[38] Zhang J., Yan S., Fu L., Wang F., Yuan M., Luo G., Xu Q., Wang X., Li C., Photocatalytic Degradation of Rhodamine B on Anatase, Rutile, and Brookite TiO_2, *Cuihua Xuebao/Chinese J. Catal.* **32**, 983 (2011).

[39] Hedayati K., Ebrahimi Z., Ghanbari D, Preparation of Hard Magnetic $BaFe1_2O_{19}TiO_2$ Nanocomposites: Applicable for Bhoto-Degradation of Toxic Pollutants, *Journal of Materials Science: Materials in Electronics*, **28(18)**: 13956-13969 (2017).